Research Paper

EARTHQUAKE SPECTRA

Earthquake Spectra
2025, Vol. 41(5) 3949–3976

DOI: 10.1177/87552930251378227
journals.sagepub.com/home/eqs
Sage

Field characterization of areas in İskenderun affected by liquefaction during the 2023 Kahramanmaraş earthquake

Cody Arnold, EERI[1], Jorge Macedo, EERI[1], Jonathan Bray, EERI[2], Diane Moug, EERI[3], Fikret Atalay[4], Patrick Bassal, EERI[5], Chenying Liu[1], Murat Bikçe[6], and Turan Durgunoğlu[7]

Abstract

The 2023 Kahramanmaraş earthquake sequence significantly impacted southeastern Türkiye. A comprehensive field investigation of 40 cone penetration tests and 7 seismic cone penetration tests was conducted to characterize the subsurface conditions of several areas affected by liquefaction in the port city of İskenderun. The investigations were performed at a key seismic station in the area, five areas with differing liquefaction-induced building settlements, and three lateral spread sites. The reclaimed shoreline area, which exhibited the most significant liquefaction effects, is underlain by thick medium dense clean sand deposits. Ground shaking characteristics in the investigated areas are estimated and essential subsurface data for developing high-quality field case histories are developed to support studies of liquefaction triggering and effects in İskenderun. In this context, it contributes to advancing liquefaction engineering and informs seismic hazard mitigation strategies in urban areas.

Keywords

Case histories, earthquakes, lateral spreading, liquefaction, settlement

Date received: 21 November 2024; accepted: 13 July 2025

[1]Georgia Institute of Technology, Atlanta, GA, USA
[2]University of California, Berkeley, Berkeley, CA, USA
[3]Portland State University, Portland, OR, USA
[4]EGSci Consulting, Atlanta, GA, USA
[5]The Ohio State University, Columbus, OH, USA
[6]İskenderun Technical University, İskenderun, Türkiye
[7]Zemin Etüd ve Tasarım A.Ş., İstanbul, Türkiye

Corresponding author:
Jorge Macedo, Georgia Institute of Technology, 790 North Ave NW, Atlanta, GA 30332, USA.
Email: Jorge.Macedo@gatech.edu

Introduction

The 2023 Kahramanmaraş earthquake sequence produced severe damage in southeastern Türkiye and resulted in significant loss of life. Extensive evidence of liquefaction-related damage was identified by the National Science Foundation (NSF) funded Geotechnical Extreme Events Reconnaissance (GEER) teams that worked with researchers from the Middle Eastern Technical University (METU) and other engineers. This liquefaction-related damage is documented in Cetin et al. (2023) and Moug et al. (2023). In addition, Moug et al. (2024a) and Bassal et al. (2024) provide post-earthquake field observations in İskenderun of liquefaction-induced effects on 26 buildings and seven liquefaction-induced lateral spreading transects in İskenderun.

Post-earthquake reconnaissance following the moment magnitude (M_w) 7.8 Kahramanmaraş earthquake provided a remarkable opportunity to develop numerous high-quality case histories of liquefaction-induced damage in İskenderun, Türkiye. Well-documented field case histories are crucial for developing and validating methods for assessing liquefaction triggering and its consequences. This study utilized the cone penetration test (CPT) as it is the preferred method for subsurface characterization of liquefaction case histories involving primarily sand materials due to its nearly continuous profiling, accuracy, and repeatability.

This study presents CPT data collected in March 2024. The CPT profiles characterize the subsurface conditions at liquefaction-induced lateral spread transects (LS) and building settlement sites. Through this effort, 40 CPT, 7 seismic CPTs (SCPTs), and 3 soil borings were performed. Subsurface conditions are documented at 17 buildings that experienced liquefaction-induced settlements from less than 1 to 74 cm and includes three sites where building-ground interactions resulted in hogging ground deformation (i.e. when building settlement drags the surrounding earth downward) for several meters around the building. In one case, a single-story building was damaged by the ground deformation induced by adjacent taller buildings. The CPT investigations also consider seven liquefaction-induced lateral spread transects with observed accumulated deformations from 20 to 147 cm. In addition, this study provides estimates of earthquake ground motion intensity measures to characterize the seismic loading at these field case histories. CPT-based liquefaction assessment of liquefaction triggering, post-liquefaction volumetric settlement, and lateral displacement are assessed using several procedures currently used in engineering practice to provide insights. The critical layers are characterized at eight level ground sites. All geo-located field testing data reported in this study are available at DesignSafe (Macedo et al., 2025).

Liquefaction assessment procedures

The Boulanger and Idriss (2014) CPT-based liquefaction triggering procedure is used to calculate the factor of safety of liquefaction triggering (FS_{liq}) in this study. A soil behavior type index (I_c, Robertson and Wride, 1998) value $\leqslant$2.6 is used to identify soils susceptible to liquefaction. The sensitivity of the results to this threshold value was evaluated by considering a range of I_c from 2.5 to 2.7. The subsequent effects of varying I_c on the assessment of liquefiable layers, as well as liquefaction indices, are generally $\leqslant$10% as compared to the results using an I_c threshold of 2.6. The one-dimensional (1D) free-field post-liquefaction volumetric-induced reconsolidation settlement (S_v) is estimated using Zhang et al. (2002), and the lateral spreading displacement index (LDI) is estimated using Zhang et al. (2004). The liquefaction severity number (LSN) is calculated using van Ballegooy et al.

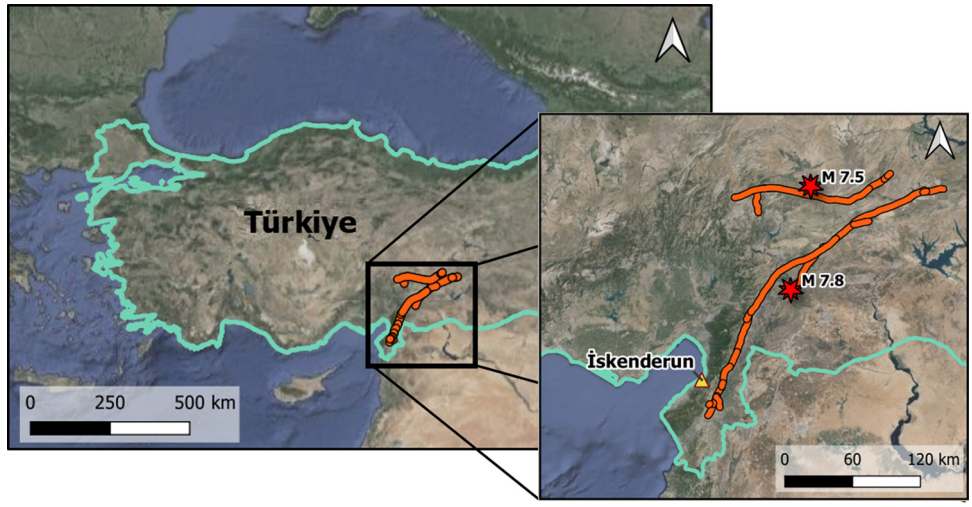

Figure 1. Location of event epicenters in relation to EAFZ and İskenderun.
Source: Base map: Google (n.d.), Faults: Reitman et al. (2023).

(2014), the liquefaction demand parameter (L_D) is calculated using Hutabarat and Bray (2022), which can be used to estimate ejecta-induced settlement using Bray and Olaya (2023), and the liquefaction building settlement index (LBS) is calculated using Bray and Macedo (2017).

2023 Kahramanmaraş earthquake sequence

Geological and tectonic setting

Türkiye is located at the junction of the Eurasian, African, Anatolian, and Arabian tectonic plates. The East Anatolian Fault Zone (EAFZ) surrounds a roughly 700 km long strike-slip fault that runs southwest to northeast in southeastern Türkiye. On February 6, 2023, Türkiye experienced two major left-lateral earthquake events along the EAFZ followed by numerous aftershocks, which is referred to as the Kahramanmaraş earthquake sequence. The first event had an M_w of 7.8 and occurred in the Pazarcık section of the EAFZ. This rupture included surrounding fault segments (e.g. Amanos and Erkenek faults). The second event had an M_w of 7.5 and occurred 9 hours after the initial event along the Çardak and Doğanşehir faults within the EAFZ. As shown in Figure 1, the first event occurred along a northeast-southwest alignment, and the second event along a west-northeast alignment. The M_w 7.8 and M_w 7.5 earthquakes had focal depths of 8.6 and 7.0 km, respectively. Figure 1 also shows the relative locations of these fault ruptures to İskenderun.

İskenderun is in the Hatay province of southeastern Türkiye. It is situated on an alluvial plain flanked by the Nur Mountain range and the Mediterranean Sea. Much of İskenderun is near sea level and has a history of flooding as well as earthquakes. Historically, the area around İskenderun has been described as swampy, indicating a high groundwater level (GWL) and poor drainage conditions. City development efforts in the twentieth century focused on draining and filling low-lying areas and extending the shoreline (Nalça, 2018). Using historical maps compiled by Nalça (2018), Moug et al. (2024a) interpreted the extent

of the reclaimed shoreline, which will be discussed later. Moug et al. (2024a), using field reconnaissance, and Taftsoglou et al. (2023), using satellite imagery, noted most liquefaction manifestations from the 2023 Kahramanmaraş earthquake occurred within the reclaimed shoreline area of İskenderun.

Previous investigations in the İskenderun area give some insight into the underlying subsurface conditions. Eryılmaz and Eryılmaz (2003) sampled shallow sediments in İskenderun Bay and observed that the recent surface sediments typically consist of sandy materials in approximately the upper 15 m, underlain by silty (silts and sandy silts) and muddy materials (with interbedded clays) to a depth of approximately 40 to 70 m. Özdemir et al. (2019) conducted Vertical Electrical Sounding (VES) surveys in the İskenderun area and estimated that Quaternary-aged alluvium extends to a depth of roughly 40 m and is underlain by various rock formations. However, none of the tests performed by Özdemir et al. (2019) or Eryılmaz and Eryılmaz (2003) were located within the reclaimed shoreline where most liquefaction evidence was observed. A micro-zonation study by Denge Mühendislik Ltd. Sti. (2011), included borings to 30 m depth with Standard Penetration Test (SPT), test pits, laboratory tests, and surface seismic surveys, showed the presence of gravels, sands, silts and clays in the upper 30 m; the sand fraction was observed to increase in areas closer to the shoreline. The Denge Mühendislik Ltd. Sti. (2011) report also documented a shallow GWL between 1.4 and 2 m depth in the explorations closest to the İskenderun shoreline.

Earthquake ground motions

Figure 2a shows the seismic strong motion stations in the vicinity of İskenderun and the 2023 rupture of the East Anatolian Fault provided by Wang et al. (2023). The closest stations to İskenderun are TK-3112; TK-3115 and TK-3116, as labeled in Figure 2b. Figure 3a presents the shear wave velocity (V_s) profiles for these stations, with time-averaged shear wave velocity values over the top 30 m (V_{s30}) reported as 233, 424, and 870 m/s, respectively (METU Earthquake Engineering Research Center).

Seismic station TK-3112 is located 2 km west of the Çay District of İskenderun (Figure 2b). Of the nearby seismic stations, TK-3112 is at a site most representative of the subsurface conditions in the study areas. A SCPT was advanced at TK-3112 to measure V_s; its data are shown in comparison to those from METU EERC in Figure 3a. Figure 3b illustrates the 5%-damped acceleration response spectra of the East-West horizontal component of the recorded motions from the M_w 7.8 mainshock at these stations. Acceleration, velocity, and displacement time histories are also shown. The recording at TK-3112 stopped early during the M_w 7.8 event, likely before the strongest shaking, so response spectra are not provided for this station.

The V_s profile at station TK-3116 (with values exceeding 800 m/s) indicates these records can be considered rock motions. The recordings at the TK-3115 and TK-3116 stations show peak ground acceleration (PGA) values ranging from 0.15 g to 0.25 g and cumulative absolute velocity (CAV) values ranging from 1.5 g·s to 3.0 g·s, which are significant. For context, the highest CAV values recorded during the 2010–2011 Canterbury earthquake sequence was below 3.0 g·s (Bray and Macedo, 2017). The peak ground velocity (PGV) values from the M_w 7.8 event are also significant (i.e. 35–50 cm/s).

Figure 4 shows CPT data near the station TK-3112; there is a thin layer of very stiff material to 1.2 m depth but given that it is thin and close to the surface, it is likely

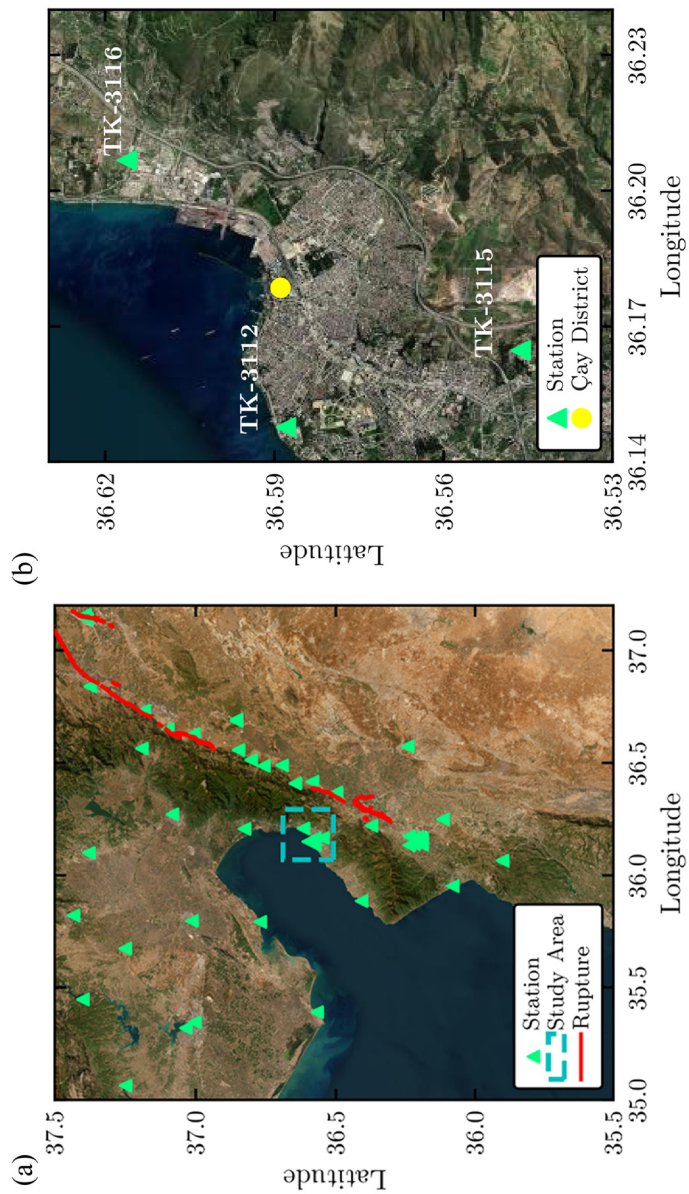

Figure 2. Locations of seismic stations and fault ruptures for the M_W 7.8 Kahramanmaraş earthquake in the İskenderun region: (a) stations within 100 km of İskenderun, and (b) stations close to the study areas. Fault rupture geometry is from Karabacak et al. (2023).

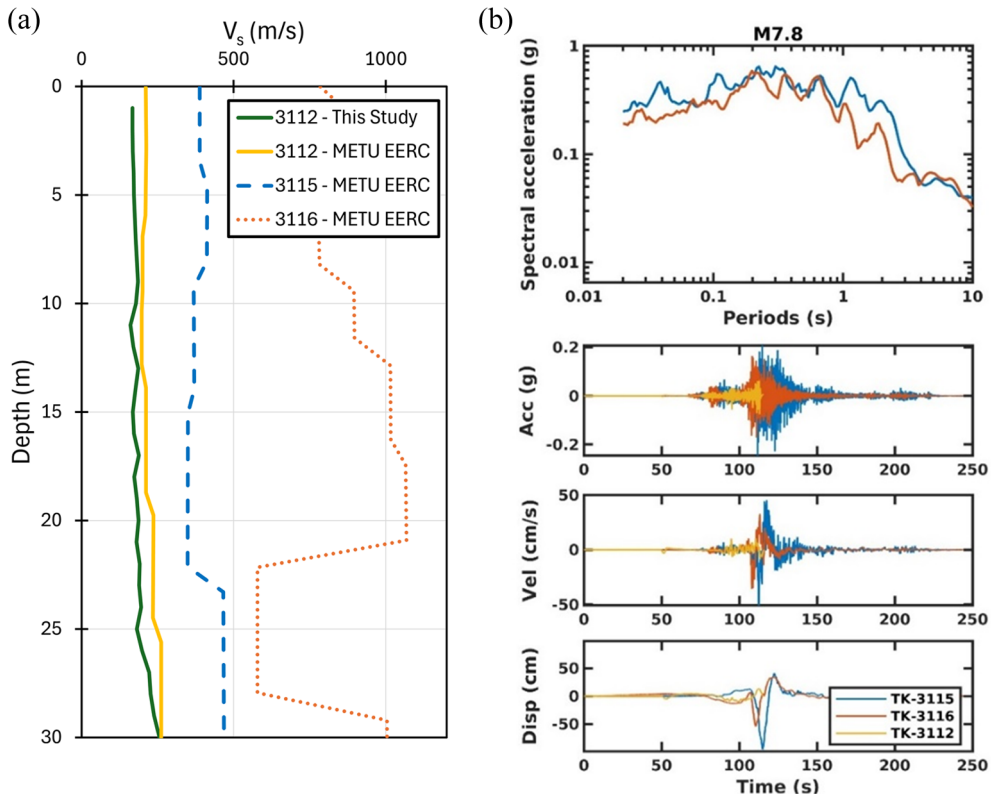

Figure 3. (a) Shear wave velocity (V_s) profiles for stations TK-3112; TK-3115 and TK-3116. (b) Ground motion time histories and 5%-damped acceleration response spectra for these stations. The M_w 7.8 earthquake was recorded fully at TK-3115 and TK-3116 and terminated early at TK-3112.

construction debris. A stratified silty-clayey layer, with a normalized friction ratio (F_r) that fluctuates between 1% and 10%, extends to a depth of 2.8 m. This is followed by a medium dense sand, with a normalized cone tip resistance (Q_{tn}) (Robertson, 2009) of 130 to 150, that extends to a depth of about 4 m. A stiff layer ($Q_{tn} \geqslant 400$; F_r around 0.5%) of gravelly sand to sand is encountered from 4 to 5 m, after which loose to medium dense sand and silty sand (Q_{tn} between 50 and 100) extend down to about 14.5 m. From 14.5 m until the end of the sounding at 30 m, clay ($I_c > 3$) with $Q_{tn} \leqslant 5$ and $F_r \sim 2.5\%$ exists. The GWL is estimated to be at a depth of 1.5 m at the time of the earthquake, as discussed later.

The V_s measurements (shown in Figure 3a and 4) indicate $V_s \leqslant 200$ m/s above 25 m in depth, below which the V_s begins to increase to about 250 m/s. The V_s values measured in this study are about 20% lower than the METU values (Figure 3a). The V_{s30} based on the SCPT-measured V_s profile in this study is 186 m/s, instead of 233 m/s as reported by METU based on data collected using ReMi and MASW tests.

Ground motion records from Buckreis et al. (2024) were used to estimate intensity measures for the M_w 7.8 earthquake at the study sites. The BSSA14 Ground Motion Model (GMM, Boore et al., 2014) and the algorithm proposed by Jayaram and Baker (2010) were employed to estimate the within-event residuals of the M_w 7.8 Kahramanmaraş earthquake. An empirical semi-variogram was estimated based on these within-event residuals

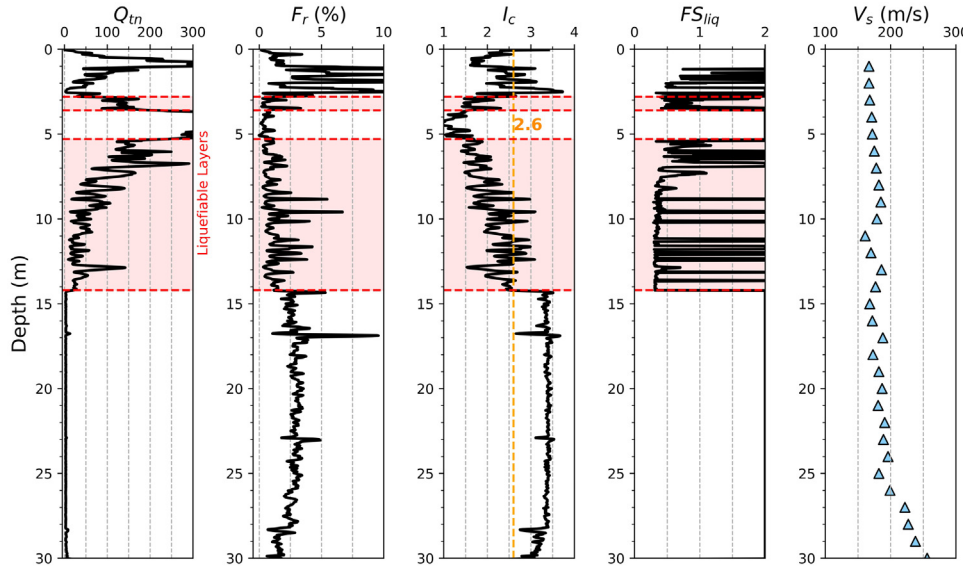

Figure 4. Normalized CPT readings (Q_{tn} and F_r) at SMS TK-3112 (SCPT63) with calculated I_c and FS_{liq}, and measured V_s.

Table 1. Earthquake ground motion parameters at key areas (median and 16–84% percentiles in brackets).

Site	PGA (g)	Sa(1s) (g)	CAV (m/s)
Area 1	0.33 [0.27–0.41]	0.64 [0.52–0.78]	26 [21–32]
Area 2	0.33 [0.27–0.41]	0.66 [0.54–0.79]	26 [21–32]
Area 3	0.32 [0.26–0.39]	0.65 [0.53–0.79]	26 [21–32]
Area 4	0.32 [0.28–0.37]	0.65 [0.57–0.74]	26 [21–30]
Area 5	0.32 [0.28–0.37]	0.65 [0.57–0.74]	26 [21–30]

and fitted using an exponential variogram model. This fitted variogram model was used to interpolate the within-event residuals. The interpolated within-event residuals, combined with the between-event residuals and the median intensity measures estimated by the BSSA14 GMM, were used to generate maps of intensity measures. This approach, known as kriging, is consistent with the methodologies used by Jayaram and Baker (2009) and Bradley and Hughes (2012).

The interpolated maps of intensity measures and their residuals are presented in Figure 5 for PGA, Spectral Acceleration at 1 second (Sa(1s)), and CAV, respectively. The PGA, Sa(1s), and CAV values at the study sites were extracted from these maps. The study sites are grouped into five areas for building settlement investigations: Areas 1 through 5 and seven lateral spread transects: LS1 through LS7, as shown in Figure 6. Considering representative V_{s30} values of 226, 201, 193, 193, 193, and 185 for Areas 1, 2, 3, 4, 5 and seismic station TK 3112, respectively, and V_{s30} values from Okay and Özacar (2023) for other locations. The estimated median PGA, Sa(1s), and CAV values (with 16% and 84% values) are reported in Table 1. These values are used for triggering liquefaction assessments and settlement estimations in later sections of this paper.

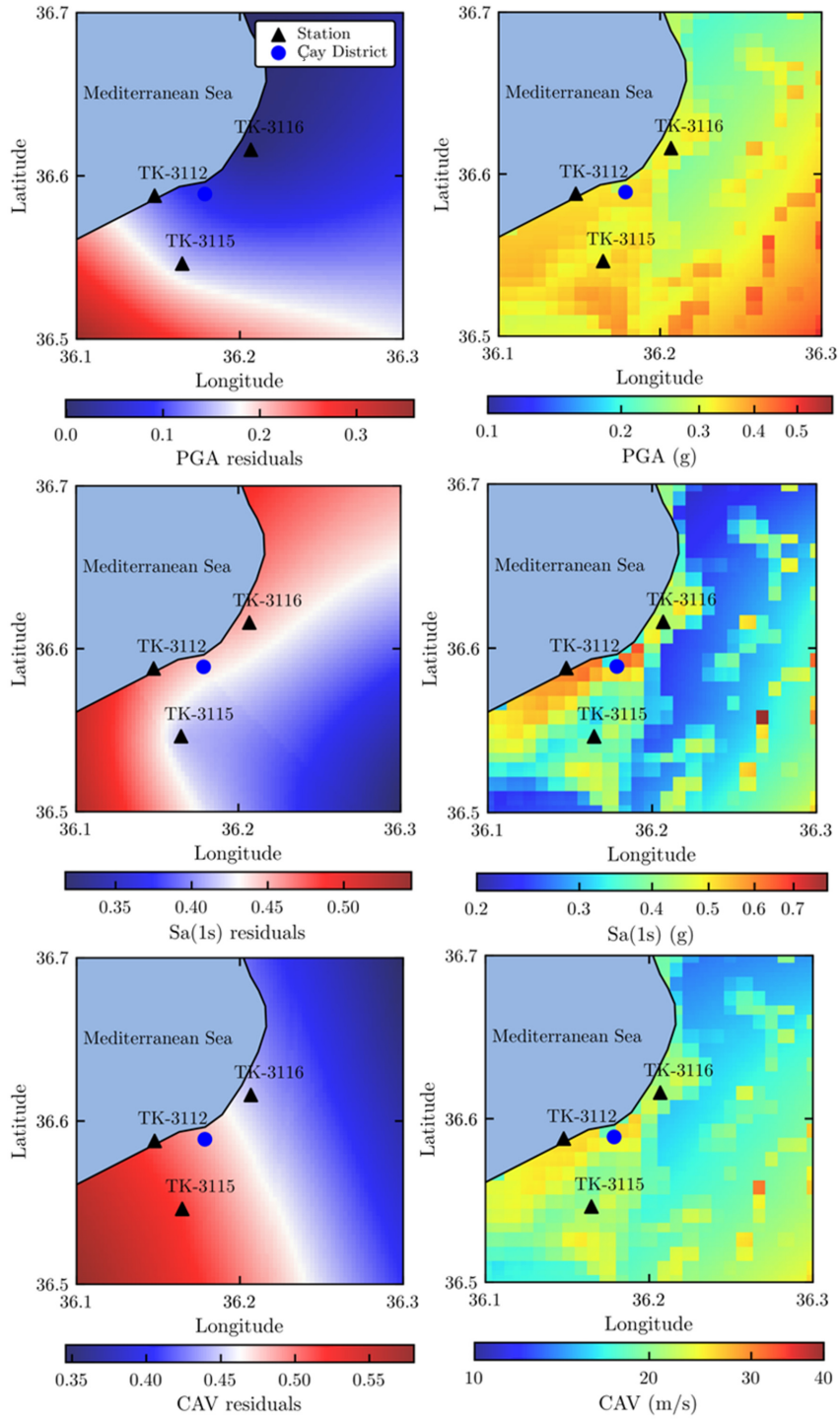

Figure 5. Maps of intensity measures and residuals estimated using kriging for the M_w 7.8 Kahramanmaraş earthquake in the areas of interest within the İskenderun region.

Figure 6. Overview of liquefaction observations and demarcation of key study areas within İskenderun.

Figure 7. Examples of (a) ejecta along Atatürk Boulevard (delineated in Figure 6) after the M_w 7.8 earthquake, (b) lateral spreading toward seawall at LS4 site, and (c) liquefaction-induced building settlement near Area 1 (from Cetin et al., 2023).

Overview of liquefaction-induced damage in İskenderun

Post-earthquake reconnaissance (e.g. Cetin et al., 2023; Moug et al., 2023) found most of the liquefaction-induced damage was located within the reclaimed areas along the current shoreline (Figure 6). Significant volumes of ejecta were observed covering Atatürk Boulevard (Figure 7a), which is the main roadway near the shoreline and generally aligns

with the historic shoreline and boundary of reclaimed land; little ejecta was observed south of Atatürk Boulevard, except for the Çay District where land reclamation extended further inland.

Moug et al. (2024a) and Bassal et al. (2024) reported ranges of liquefaction-induced settlements from less than 1 to 74 cm and lateral spreading up to 147 cm within the reclaimed areas along the shoreline. Settlement was captured using terrestrial lidar scans and laser-level hand surveys. Moug et al. (2024a) observed the building-ground interaction mechanism of hogging in many of these areas. Lateral spread displacements, which mostly occurred along the seawall within the reclaimed areas (e.g. Figure 7b), were measured by Bassal et al. (2024) via direct measurement of crack widths. Frequent floods affected the shoreline area during high tides and storm events in the months after the earthquakes, which have been attributed to liquefaction-induced free-field settlement and lateral spreading, damage to flood protection systems, and ongoing regional subsidence (e.g. Bassal et al., 2024; Öztürk et al., 2024).

Site investigation overview

The 47 CPT soundings, seven of which were SCPT, were conducted per ASTM D5778-07 using a 10 cm^2 A.P. van den Berg cone and a truck-mounted CPT rig. Only the results from the soundings relevant to the selected study areas are presented in this paper. In addition, three soil borings were performed for soil sample collection for use in future laboratory tests. The CPT investigations considered the five building settlement areas and seven lateral spread transects shown in Figure 6. At times, the locations of the CPTs had to be moved away from buildings or lateral spreads due to underground utilities and access restrictions. Most of the CPTs had to be pre-drilled to depths of 1.5 to 4.5 m due to the presence of the upper gravelly fills in the investigation areas. The difficulty in advancing the CPT and to drill through the gravelly fills indicated they were dense. SPTs by Özener et al. (2024) indicate a median overburden corrected blow count $(N_1)_{60}$ of 30 in the gravelly fill after estimating energy by comparing SPT blow counts in sand with the CPT data collected in this study. The CPTs generally extended to a depth of 30 m below the ground surface, while a few CPTs extended deeper to a maximum depth of 43.5 m; 1,509 m of CPT soundings were performed in this investigation.

The depth of the GWL was measured in the pre-drilled holes. Porewater dissipation tests were also performed at selected intervals in most soundings to cross-check the groundwater levels and to obtain porewater dissipation data. The GWL was measured to be close to 1 m in most areas, but considering post-earthquake ground settlement, the pre-event GWL depth is estimated to be about 1.5 m, which aligns with values in Denge Mühendislik Ltd. Sti. (2011). This value is used in subsequent analyses.

The subsurface conditions along the İskenderun shoreline are similar with some important variations. Figure 8 provides representative CPTs from several areas highlighted in Figure 6 to display the characteristics of CPT readings along the İskenderun shoreline area. For instance, Area 1 (CPT29), LS1 (CPT15), and LS4 (CPT47) are all within the reclaimed shoreline but are in the east, west, and center of the study area, respectively. TK-3112 (SCPT63), Area 3 (SCPT39), and Area 4 (CPT42) represent the ground characteristics within the historic land boundary and are in the west, center, and center of the study area, respectively. As shown in Figure 8, CPTs conducted within the reclaimed land typically required significant pre-drilling to bypass gravelly fill that extended to a depth of

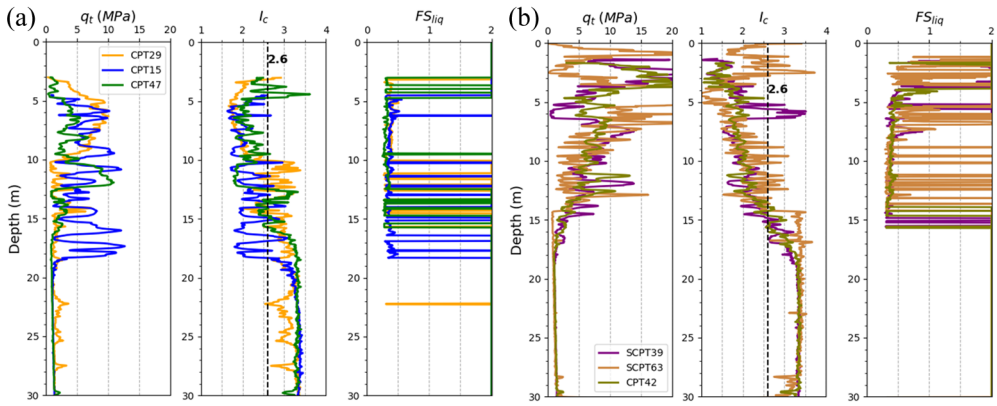

Figure 8. CPT-measured q_t with calculated I_c and FS_{liq} for specific areas highlighted in Figure 6 to show general conditions and variability: (a) areas located within reclaimed shoreline, and (b) areas within historical land boundary.

3 m on average. CPTs conducted outside of the reclaimed shoreline (i.e. within the historic land boundary) did not require significant pre-drilling.

The general CPT response throughout İskenderun indicates a predominantly sandy layer, identified by I_c values between 1.3 and 2.2, which is fairly consistent within the reclaimed land but noticeably denser in those areas within the historic land boundary (e.g. Area 3, SMS 3112, and Area 4). Within the eastern portion of reclaimed land (including Areas 1 and 2, and LS 5, 6, 7) the sand layer is underlain by an interbedded zone of sandy silts to clayey silts which ultimately transitions toward more homogeneous silty clay with some thin seams of sand and silt. To the west within the reclaimed land (i.e. LS 1, 2, 3 and 4), the upper sand layer becomes thicker, extending to approximately 12 m, and the interbedded zone becomes sandier, in some cases extending up to 18 m in depth. CPTs soundings within the historic land boundary generally indicate denser sandy silt to sand in the upper 3 m, followed by sand to silty sand to a depth of 15 m, which is typically underlain by silts and clays.

Subsurface characterization at building settlement sites

Area 1

Area 1 is located within the reclaimed shoreline in the Çay District of northeast İskenderun, as shown in Figure 6. It includes four buildings: Buildings G, H, I and J. The layout of the buildings and CPT explorations in this area is shown in Figure 9, with CPT profiles shown in Figure 10. The building plans indicate the four 6-story buildings are constructed from reinforced concrete (RC) frames with infill walls (RCF-IW) and feature a salon-type first floor (having an open ceiling to the second floor on one side). The buildings are depicted as having 2.5 m deep basements based on their architectural drawings (as shown in Figure 11). This is a common construction method in İskenderun for buildings of this size (Moug et al., 2024a). The building foundations consist of two design types. Buildings J and G apparently have a 50-cm thick RC mat overlain with 1 m deep intersecting beams that form a grid, wherein the cells are filled with compacted earth and a

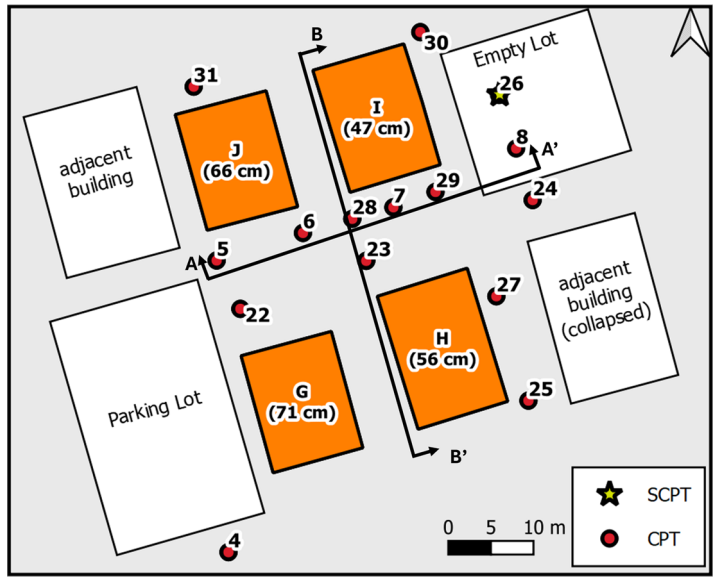

Figure 9. Overview of Area 1 with CPT and SCPT locations as well as observed building settlements measured by Moug et al. (2024a).

concrete cap slab. In contrast, Buildings I and H apparently have only 50 cm slabs with no crossbeams.

In Area 1, 14 CPTs and 1 SCPT were performed. Material presumed to be fill due to the presence of debris and cobbles was encountered in the upper 3 to 4.5 m. This upper material could not be penetrated with the CPT due to its density and large particles and objects; therefore, pre-drilling was performed to depths ranging between 3 and 4.5 m in this area. As shown in Figure 11, this corresponds to the base of the foundation indicating that the subsequent estimations of LBS, S_v, LSN, and L_D, as outlined in the Liquefaction Assessment Procedures Section, are unaffected by the pre-drilling. Figure 10 shows that the fill is underlain by a predominately sandy layer that extends to about a depth of 10 m.

The sand unit is characterized by Q_{tn} between 75 and 120 and an average I_c of 1.8. Beneath the sand unit is an interbedded sandy silt and silty clay unit exhibiting lower Q_{tn} ($\leqslant$35) and a fluctuating I_c between 2.4 and 2.9, which transitions into a clay unit below 14.5 m. V_s increases from about 200 m/s to 250 m/s over the depth of the sounding (Figure 10). Figure 11a and 11b show these stratigraphic units considering the North-South (Figure 11a) and East-West (Figure 11b) directions. The CPT profiles in this area are remarkably uniform; therefore, variable liquefiable unit thickness was not considered for the liquefaction assessments.

Simplified liquefaction assessments were carried out using the procedures described previously. Based on the subsurface conditions, the upper sand unit from 3 to 10 m is liquefiable (Figures 10 and 11). In addition, there are thinner layers of potentially liquefiable material in the looser interbedded zone from 10 to 15 m. As discussed previously, the pre-event GWL depth is estimated to be about 1.5 m in the analyses. As shown in Figure 9 the observed building settlements range from 47 to 71 cm, which are largely from the shear-induced component of liquefaction-induced building settlement (Bray and Macedo, 2017).

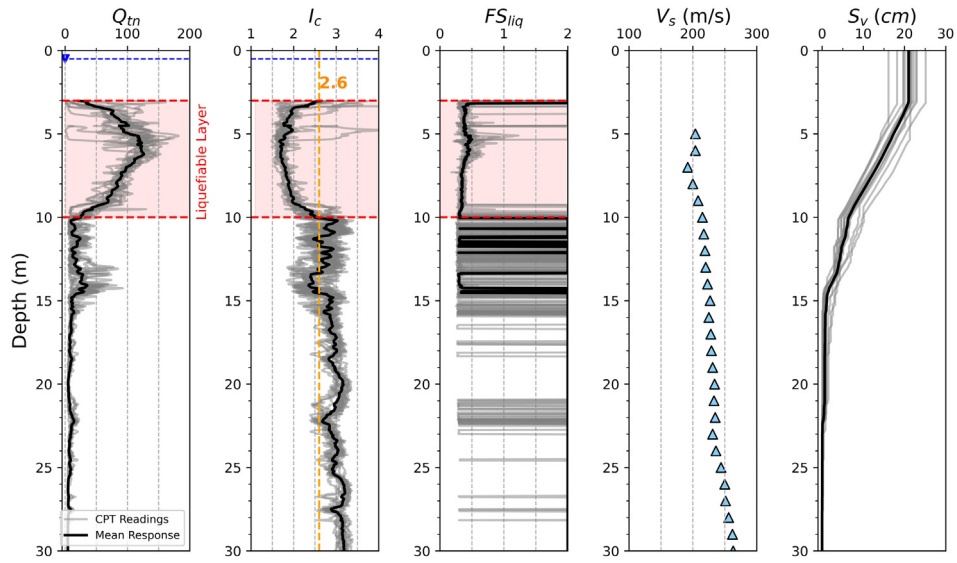

Figure 10. Range of normalized CPT readings (Q_{tn}) at Area 1 with calculated I_c, FS_{liq}, and S_v profiles, and V_s measurements. Soil unit with $FS_{liq} < 1.0$ is denoted as the liquefiable layer.

LBS is used as an index of performance of the shear-induced building settlement component. For the ejecta-induced building settlement component, LSN and LD are used as indices of ejecta potential. The free-field ground surrounding the buildings as well as the buildings also settled due to 1D post-liquefaction volumetric strain (S_v). The range of estimated S_v values shown in Figure 10 are 16 to 25 cm. Estimated 16% to 84% ranges of the liquefaction indices for Area 1 are LBS from 23 to 35, LSN from 25 to 33, and L_D from 40 to 80. L_D was found to be sensitive to the unit weight of the drilled-out fill. The fill material is assumed to have a unit weight of 20 kN/m^3 based on its field description. In Area 1, L_D = 40 to 80 indicates ejecta to be severe with an estimated localized free-field ejecta-induced settlement of 3 to 20 cm.

Area 2

Area 2 contains three buildings in the Çay District which are about 75 m west of Area 1. It is also located within the reclaimed shoreline. The group of buildings consists of two RCF-IW buildings (K and M) with a 1-story steel-frame building (L) on a concrete slab foundation between them (Figure 12). Building plans for Buildings K and M depict similar construction as Area 1 with salon-type first floors. Building M is 6 stories with a partial seventh floor as well as a 2.5-m deep basement on a 30-cm thick slab. Building K is a 5-story structure with a 2-m deep partial basement that does not extend across the full building footprint.

Four CPTs and one SCPT were performed along Atatürk Boulevard at the corners of buildings M and K, and one additional CPT was located at the rear corner of building M, as shown in Figure 12. Prior to the CPT soundings, 3 m of pre-drilling was performed to bypass the upper dense gravelly fill. The subsurface conditions shown in Figure 13 are like those of Area 1. The sand unit beneath the fill has similar Q_{tn} (75 to 120) and I_c (1.8)

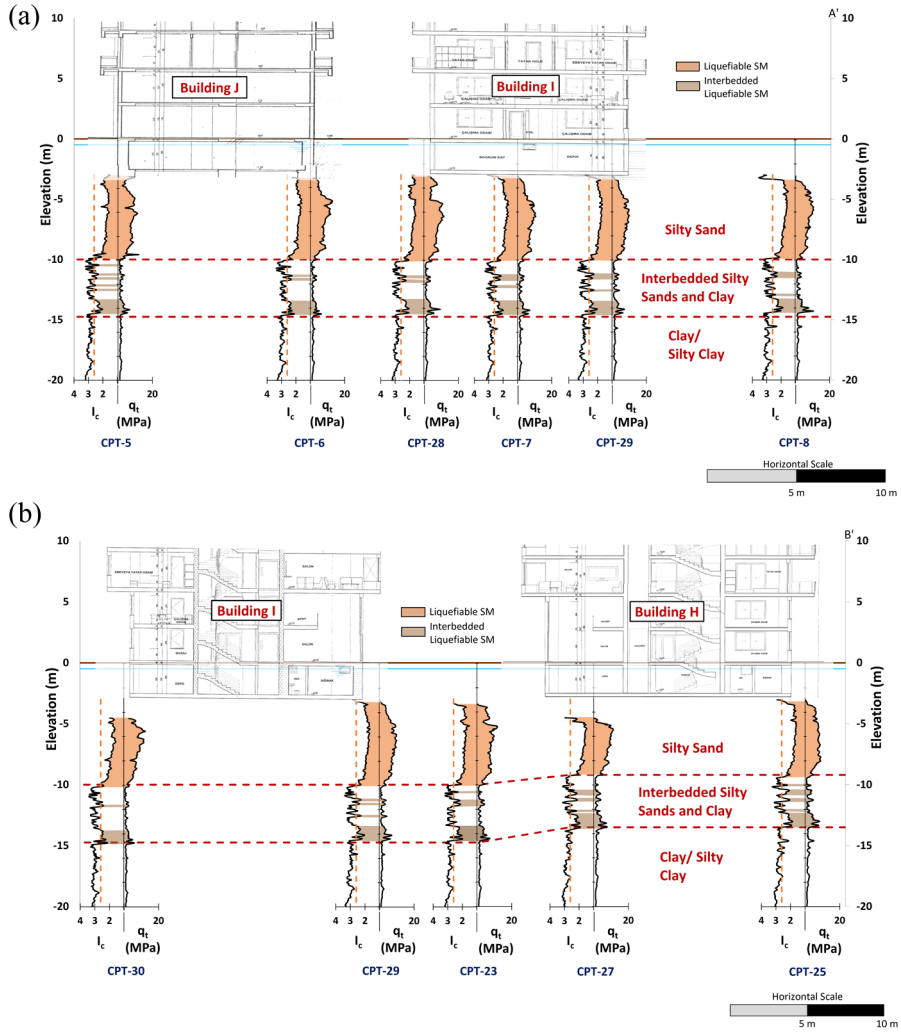

Figure 11. Cross-sections (a) A-A′ across buildings J and I and (b) B-B′ Buildings I and H (only first 3 stories of building plans shown) from Figure 9.

values as those of Area 1. The interbedded sandy silt and silty clay unit below the sand has fewer layers of liquefiable material compared to Area 1 due to its higher I_c values; its Q_{tn} ($\leqslant$15) is lower than the sand layer above it. The deeper clay unit is like the same unit in Area 1 and is characterized by $Q_{tn} \leqslant 15$ and $I_c \geqslant 3$. V_s fluctuates between 180 and 220 m/s over the depth of the sounding. A geotechnical section across buildings M, L (not shown), and K (Figure 14) indicates the subsurface conditions are uniform.

The range of estimated S_v values depicted in Figure 13 are between 16 and 22 cm. LBS, LSN, and L_D have 16% to 84% ranges of 23 to 31, 27 to 30, and 55 to 110, respectively. These values are consistent with those estimated for these indices in Area 1. The observed settlements of 38 cm and 51 cm of the taller buildings K and M, respectively, in Area 2 (Moug et al., 2024a) are lower than those observed in Area 1 (i.e. 47 to 71 cm). The lower building settlement could be due in part to the underlying interbedded sandy silt and silty

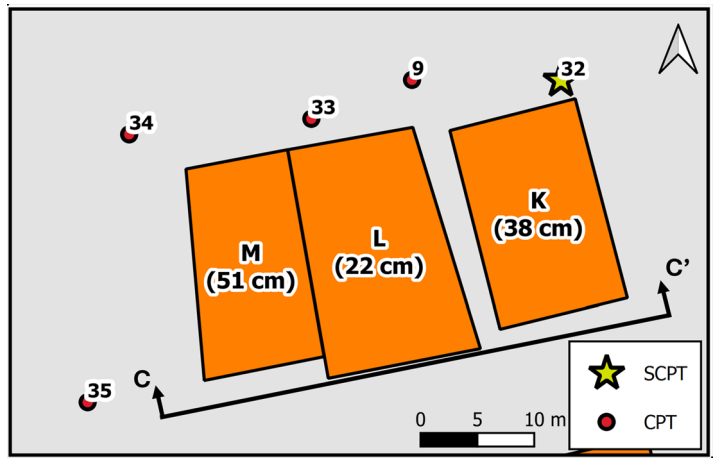

Figure 12. Overview of Area 2 with CPT and SCPT locations as well as observed building settlements measured by Moug et al. (2024a).

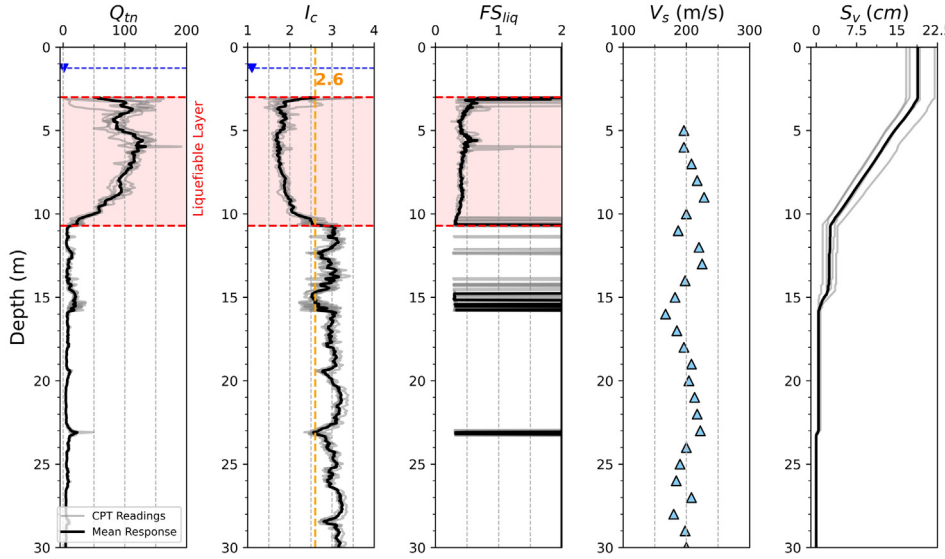

Figure 13. Range of normalized CPT readings (Q_{tn}) at Area 2 with calculated I_c, FS_{liq}, and S_v profiles, and V_s measurements. Soil unit with $FS_{liq} < 1.0$ is denoted as the liquefiable layer.

clay unit that exhibits a more fine-grained response (higher average I_c) as compared to the same unit in Area 1.

Area 3

Area 3 is in the Yenisehir neighborhood, which is about 1 km west of the Çay District (Areas 1 and 2) and is on the historic shoreline (i.e. CPTs may or may not be on reclaimed land). It contains two 6-story RCF-IW buildings (V and T) that are adjacent to the 2-story

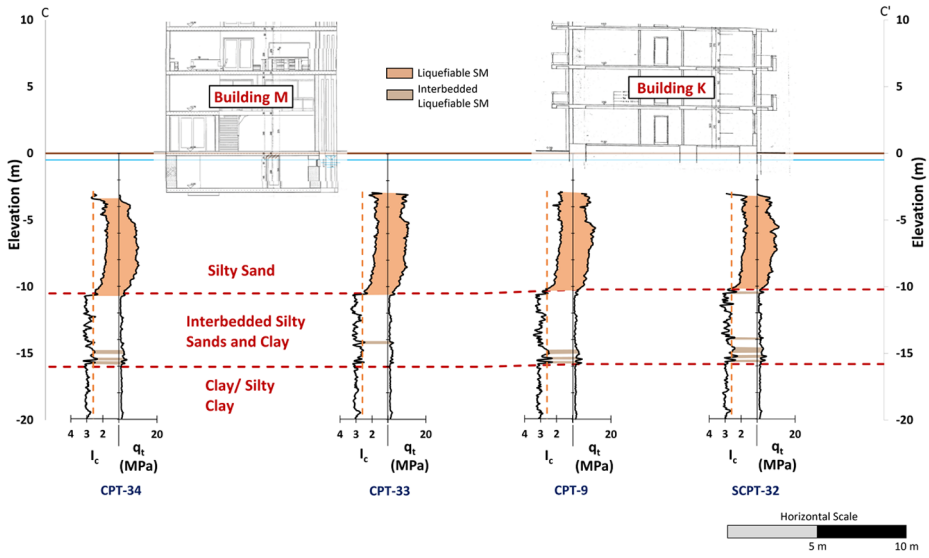

Figure 14. Cross-section C-C′ from Figure 12 of Area 2 (only first 3 stories of building plans shown for Buildings M and K; Building L (not shown) is between Buildings M and K).

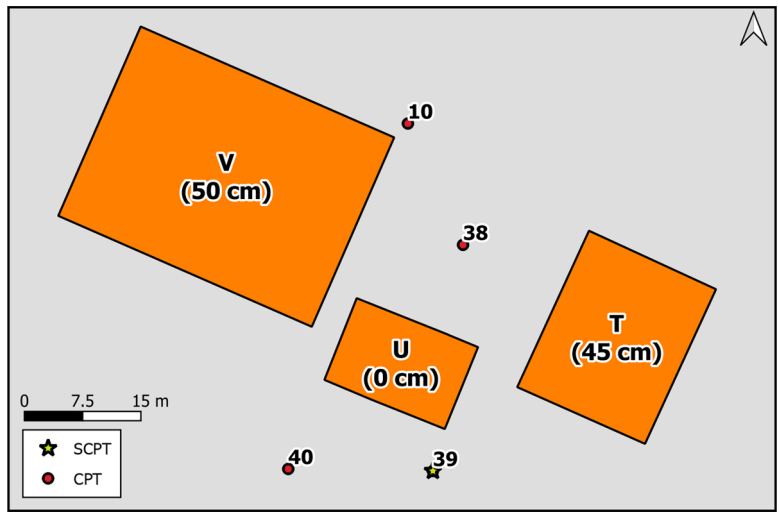

Figure 15. Overview of Area 3 with CPT and SCPT locations as well as observed building settlements measured by Moug et al. (2024a).

middle Building U (Figure 15). Plans were not available for these buildings. It is assumed that Buildings V and T are similar in construction to the Area 1 and 2 buildings described previously. Based on field observations, Building V has a basement and Building T does not have a basement.

Three CPTs and one SCPT were performed at this location: two near Atatürk Boulevard to the north of Building U and two to the south behind Building U (Figure 15).

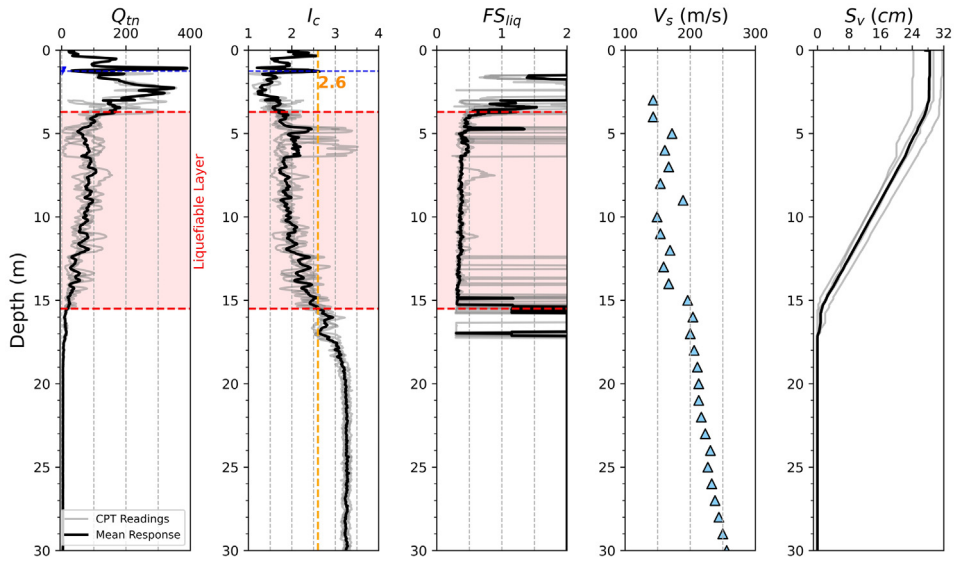

Figure 16. Range of normalized CPT readings (Q_{tn}) at Area 3 with calculated I_c, FS_{liq}, and S_v profiles, and V_s measurements. Soil unit with $FS_{liq} < 1.0$ is denoted as the liquefiable layer.

Northern CPTs required 3 m of pre-drilling, consistent with Areas 1 and 2, indicating they penetrate reclaimed land; however, the southern CPT did not require pre-drilling and the SCPT required only 1.5 m of pre-drilling. A dense sand unit ($Q_{tn} \geqslant 100$ to 300; $I_c \sim 1.3$ to 2) is present near the ground surface, extending to 3 m, which then becomes less dense ($Q_{tn} \leqslant 100$; $I_c \sim 2$) and continues to loosen ($Q_{tn} \sim 50$) to a depth of roughly 15 m. Below 15 m, the response gradually transitions from silty sand to clayey silt materials to a depth of 18 m, which is characterized by $Q_{tn} \leqslant 10$ and $I_c \sim 2.9$, after which the deeper clay unit exists with $Q_{tn} \leqslant 5$ and I_c of 3.2. This soil profile differs from those in the Çay District (i.e. Areas 1 and 2), which had a more notable interbedded soil unit starting at a depth of 10 m. The GWL was measured at a depth of about 1 m. Figure 16 shows the measured CPT profiles as well as the resulting FS_{liq}, which highlights the greater thickness of liquefiable material in Area 3 compared to Areas 1 and 2. The V_s ranges between 150 and 200 m/s for the upper 15 m of material, beneath which it gradually increases from 200 m/s to 250 m/s at a depth of 30 m.

Buildings V and T have similar amounts of building settlement (Figure 15) as observed for the taller buildings in Areas 1 and 2 (Moug et al., 2024a). However, the range of estimated S_v (24 to 32 cm) from the CPTs in Area 3 is higher than in the other areas, and the 16% to 84% ranges of LBS and LSN of 37 to 44 and 32 to 38, respectively, in Area 3 are also higher than in the other areas. The L_D values of 28 to 65 are lower than those in Areas 1 and 2 but they also indicate severe ejecta with an estimated localized free-field ejecta-induced settlement of 3 to 20 cm. The generally higher indices for Area 3 are largely due to the greater thickness of the upper sand unit, as shown in Figure 16, extending to 15 m as compared to 10 m depth in Areas 1 and 2. The observed building settlements in all three areas are similarly large, indicating similarly poor seismic performance of these buildings.

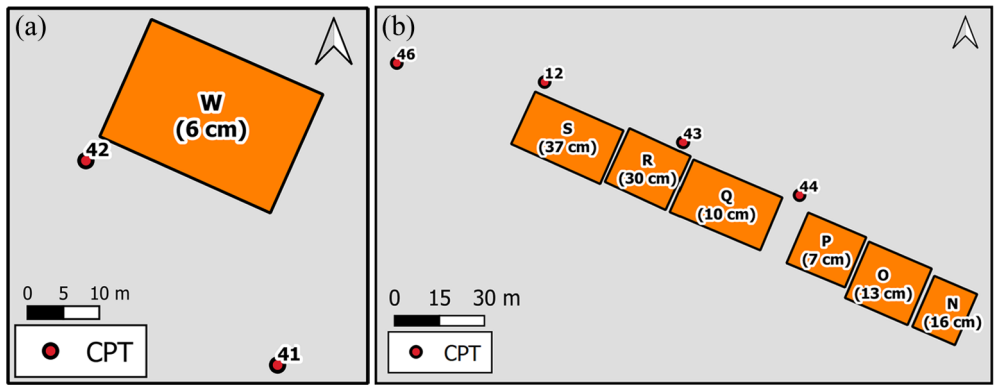

Figure 17. Overview of (a) Area 4 and (b) Area 5 with CPT locations as well as observed building settlements measured by Moug et al. (2024a).

Areas 4 and 5

Area 4 is directly south of the Buildings in Area 3, as shown in Figure 6 and 17a, and lies within the historic shoreline (i.e. not on reclaimed land). Liquefaction settlement was observed at a single 5-story building with no basement on a 50-cm thick slab. There is an empty lot on the northwest side of Building W and an adjacent building on its southeast side. Building W in Area 4 is notable as it settled only 6 cm, which is significantly less than buildings of similar size in Areas 1, 2, and 3. Area 5 consists of six buildings (S, R, Q, P, O, and N) located along Atatürk Blvd., between Areas 3 and 2, as shown in Figure 6 and 17b. Building plans were unavailable for Area 5. Buildings S, Q, and N are 7-story structures, while Buildings O and R are smaller, with 6 and 5 floors, respectively. Building P is a historic 2-story structure (Moug et al., 2024a).

Two CPTs were performed to characterize the subsurface conditions in Area 4 as shown in Figure 17a: one on the southwest corner and the other offset about 15 m from the southeast corner due to access. Both CPTs required 1.5 m of pre-drilling, which is consistent with the reduced thickness of fill seen in other areas outside of the reclaimed shoreline. Four CPTs were performed to characterize the subsurface conditions in Area 5 as shown in Figure 17b. CPTs 43, 44, and 46 were pre-drilled to a depth of 1.5 m, while CPT-12 required 3 m of pre-drilling. The CPT responses shown in Figures 18 and 19 are consistent with those of Area 3; however, with a slightly reduced thickness in the liquefiable sandy layer. The liquefiable sandy layer extends to roughly 15.5 m in Area 3, while it ends at around 14 m in Areas 4 and 5.

The values of S_v (23 and 27 cm), LBS (34 and 39), and LSN (28 and 34) calculated for the two CPTs in Area 4 are relatively consistent with those from the areas discussed previously. Despite these results, the observed settlement experienced by Building W in Area 4 is significantly lower (6 cm), which is an important aspect that warrants further study. The values of L_D (42 and 88) for Area 4 indicate severe ejecta potential, which is consistent with the other areas. The overall ranges of S_v (25 to 32 cm), LBS (40 to 62), LSN (33 to 53), and L_D (60 to 90) in Area 5 are more similar to Area 3 in that they are higher than those in Areas 1, 2, and 4. However, the buildings in Area 5 experienced a wider range of settlements (between 7 and 37 cm). Interestingly, Buildings Q, O, and N experienced significantly less settlement than Buildings S and R, despite CPT44 (which is the CPT closest to

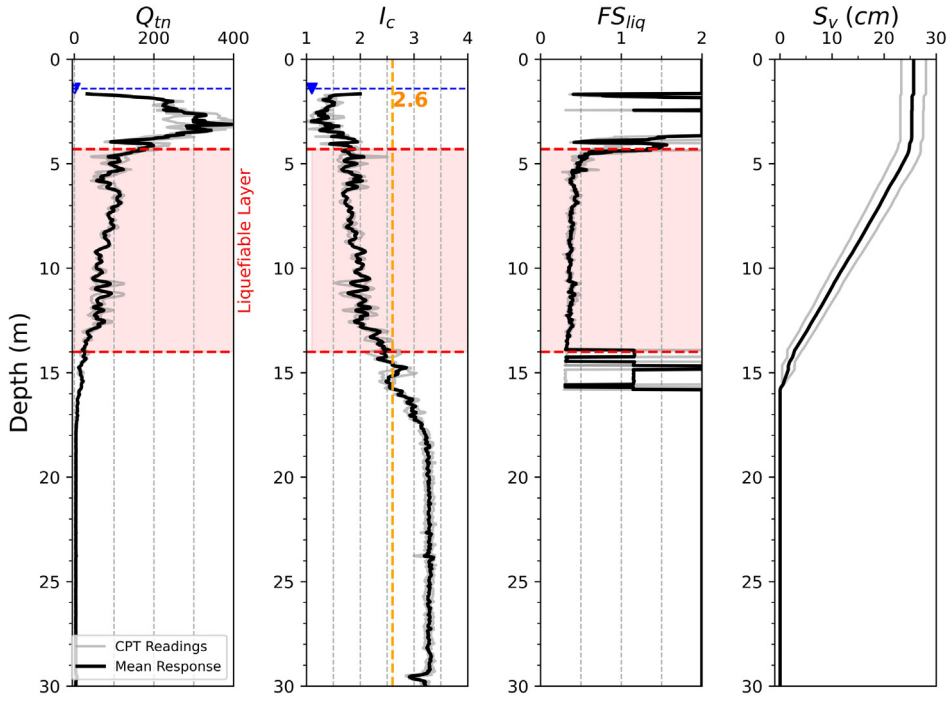

Figure 18. Range of normalized CPT readings (Q_{tn}) at Area 4 with calculated I_c, FS_{liq}, and S_v profiles. Soil unit with $FS_{liq} < 1.0$ is denoted as the liquefiable layer.

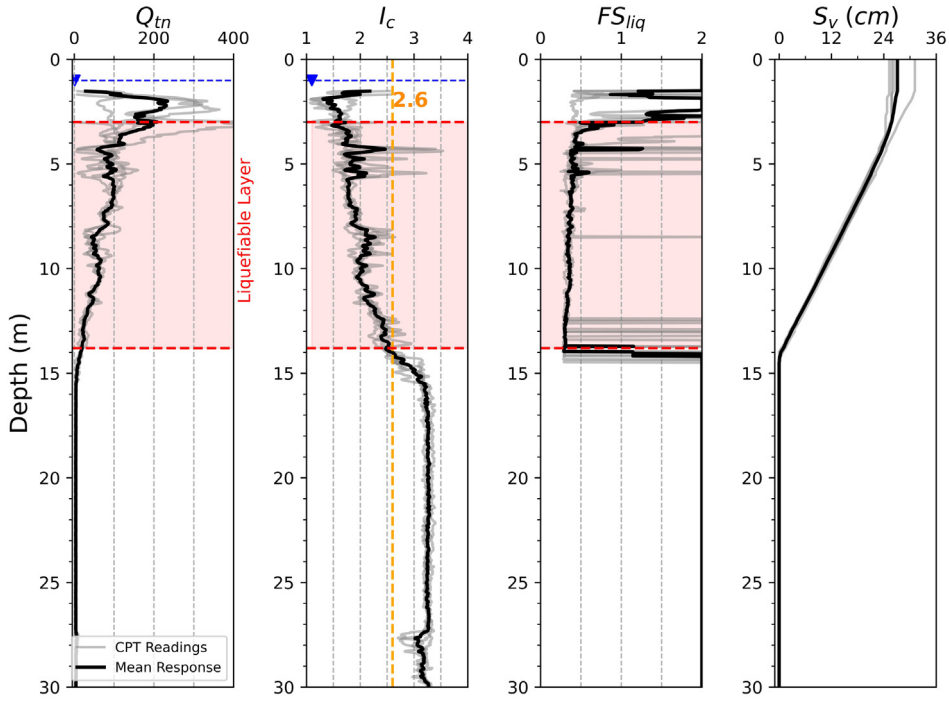

Figure 19. Range of normalized CPT readings (Q_{tn}) at Area 5 with calculated I_c, FS_{liq}, and S_v profiles. Soil unit with $FS_{liq} < 1.0$ is denoted as the liquefiable layer.

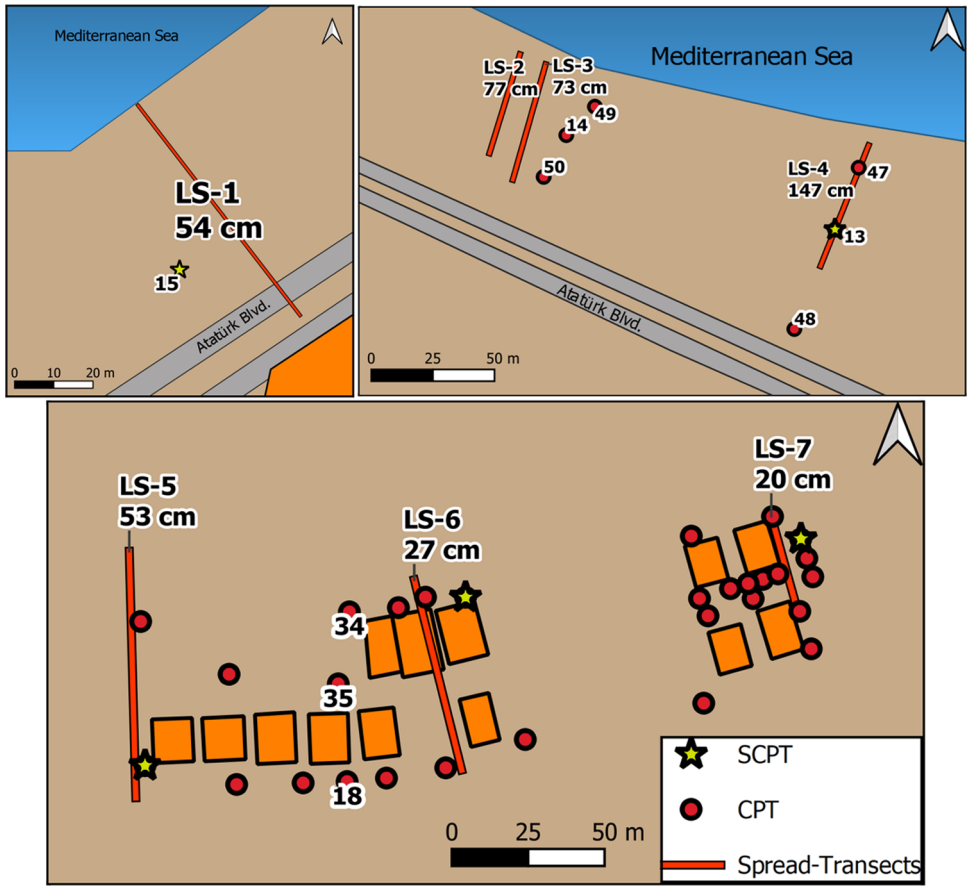

Figure 20. Layout of SCPT and CPT tests conducted to identify subsurface conditions near lateral spread transects as well as measured lateral spread distances by Bassal et al. (2024).

Buildings Q, O, and N) indicating larger S_v, LBS, and LSN values. This discrepancy could be due to various factors, including potential design differences (e.g. foundations and basements), which are currently unknown, but should be investigated in future studies.

Subsurface characterization of lateral spread sites

Bassal et al. (2024) describe the observations of lateral spreading captured from post-earthquake surveys. Seven lateral spread transects were measured in three areas of İskenderun, as shown in Figure 20. The location of the transects is also depicted in Figure 6. The seven lateral spread transects are in the reclaimed land along the current shoreline, therefore, the stratigraphy is likely represented by fill overlying alluvial deposits. All but three (i.e. LS5, LS6, and LS7) are directly behind the sea wall.

The subsurface conditions at LS1 differ from those of the other lateral spread transects (Figure 21). After 4.5 m of pre-drilling, the CPT indicates a mostly sand unit alternating with several silt layers (i.e. with $I_c > 2.6$) extending to a depth of 18 m, which is characterized by Q_{tn} ranging from 25 to 100. This unit is underlain by a predominately clay unit

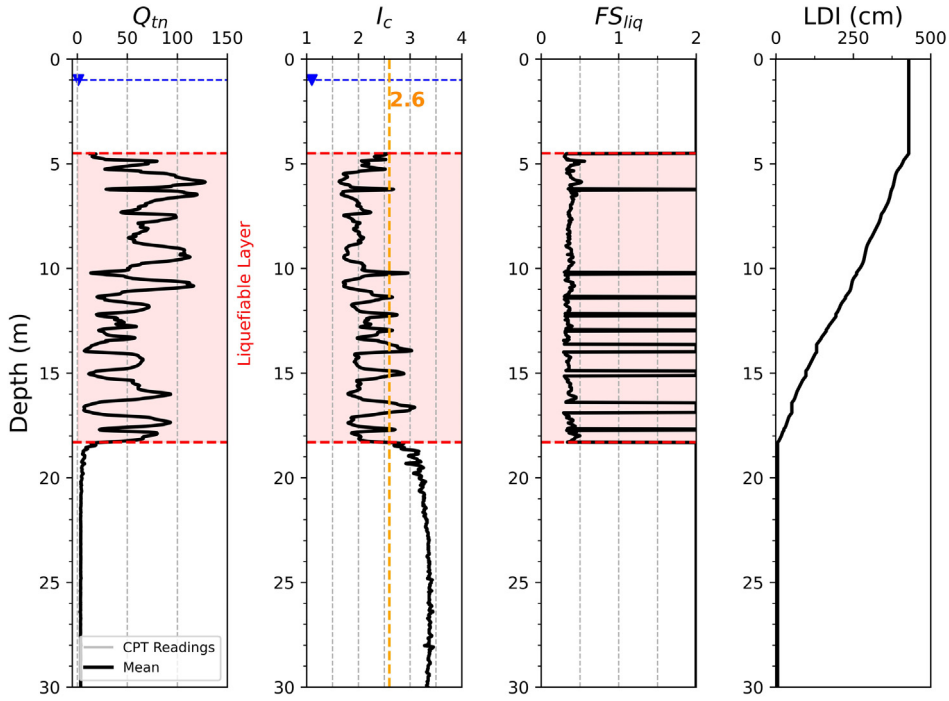

Figure 21. Normalized CPT readings (Q_{tn}) at LS1 with calculated I_c, FS_{liq}, and LDI profiles. Soil unit with $FS_{liq} < 1.0$ is denoted as the liquefiable layer.

characterized by $Q_{tn} \leqslant 5$ and I_c of 3.4. Despite these differences, the LDI values at LS1 (~420 cm) are similar to the other LS sites along the seawall, which range between 330 and 480 cm.

The LS2, LS3, and LS4 groups are within a park behind the seawall, just northeast of building settlement Area 3. Due to their proximity, LS2 and LS3 were characterized jointly by three CPTs (Figure 22), and LS4 was characterized by two CPTs and one SCPT (Figure 23). Both sets show an upper sand unit extending to a depth of 12 m, characterized by Q_{tn} of 70 and I_c ~1.9. The CPT sounding transitions into a sandy silt unit with a significantly lower Q_{tn} of 20. This is underlain by a predominately clay unit characterized by a Q_{tn} of 4 and I_c of 3.2. The resulting LDI values for the CPTs representing LS2 and LS3 (Figure 22) show consistent results within 360 to 400 cm.

In the case of LS4 (Figure 23), there is a larger variation in LDI values between CPTs of 330 cm for CPT48 to over 450 cm for CPT47. As shown in Figure 20, these CPTs had greater spacing with CPT48 being 25 m behind the most inland ground crack that was observed. This may suggest a difference in subsurface behavior that controlled the extent of lateral spreading. Despite this, the LDI results agree with estimates from other LS sites along the seawall.

The LS5, LS6, and LS7 group is within the Çay district, with LS6 and LS7 being within building settlement Areas 1 and 2. LS5 is 100 m west of LS6, but the sites show consistency in their subsurface conditions. These CPT profiles are also consistent with the nearby CPTs in Areas 1 and 2. The subsurface conditions of LS7 are captured well by the cross-section shown in Figure 11 and CPT profiles shown in Figure 10, which crosses through

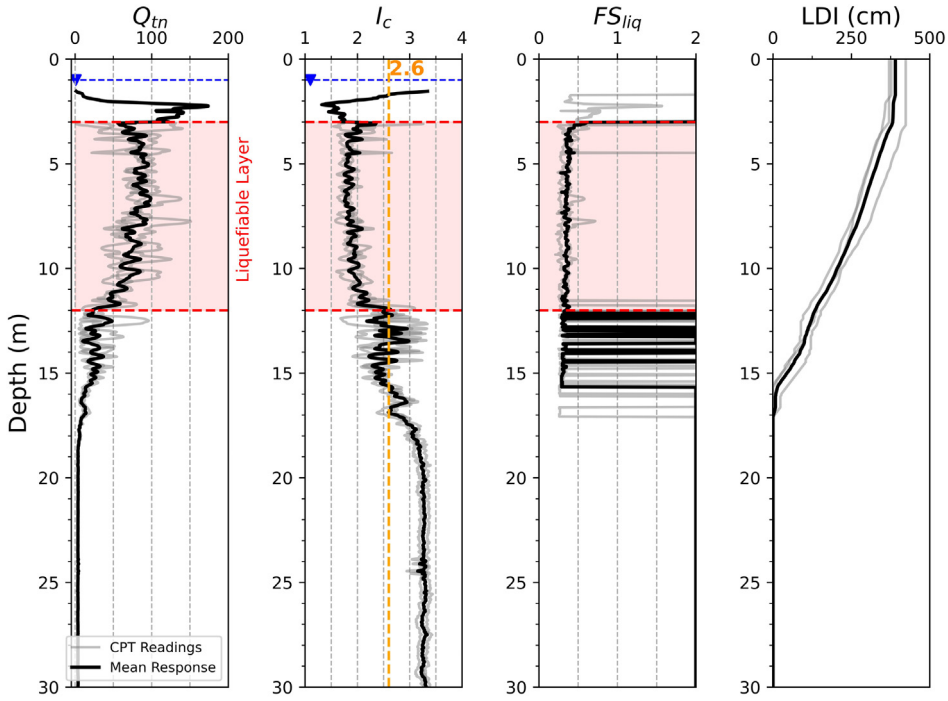

Figure 22. Range of normalized CPT readings (Q_{tn}) at LS2 and LS3 with calculated I_c, FS_{liq}, and LDI profiles. Soil unit with $FS_{liq} < 1.0$ is denoted as the liquefiable layer.

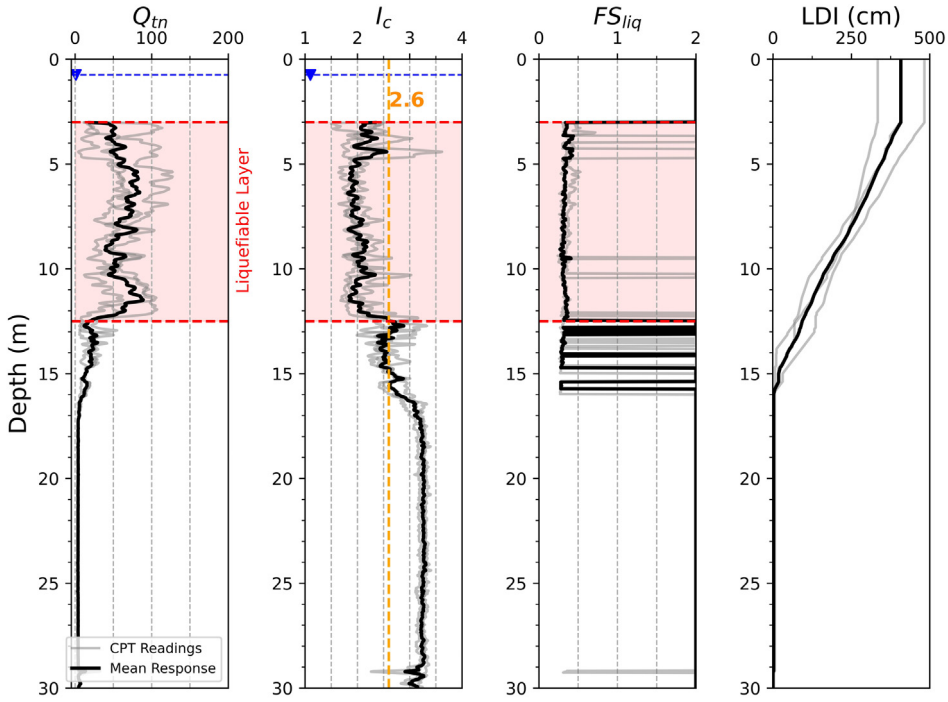

Figure 23. Range of normalized CPT readings (Q_{tn}) at LS4 with calculated I_c, FS_{liq}, and LDI profiles. Soil unit with $FS_{liq} < 1.0$ is denoted as the liquefiable layer.

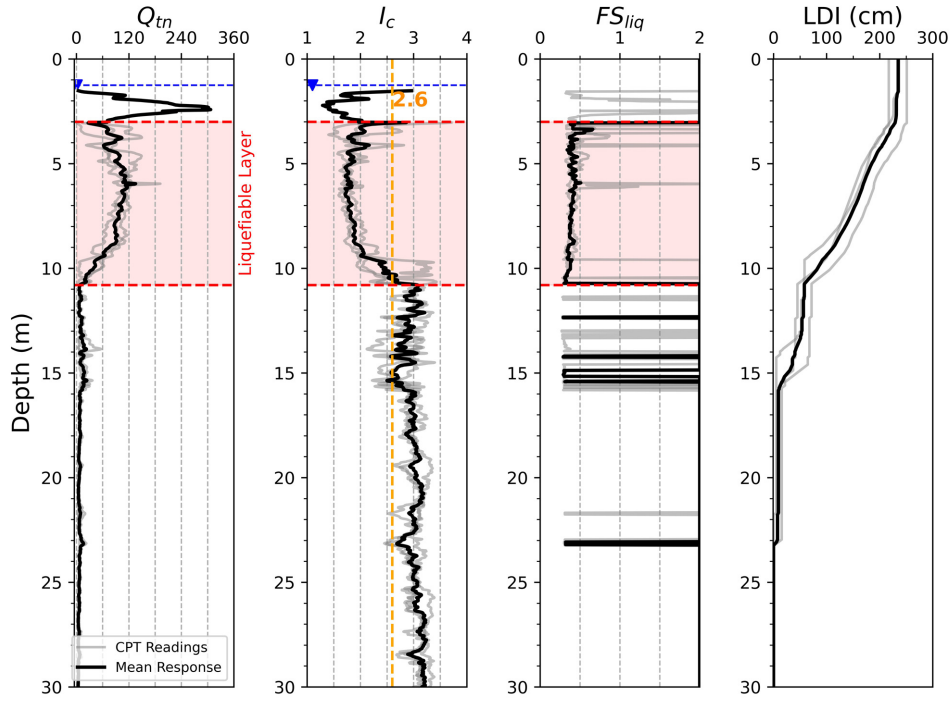

Figure 24. Range of normalized CPT readings (Q_{tn}) at LS5 and LS6 with calculated I_c, FS_{liq}, and LDI profiles. Soil unit with $FS_{liq} < 1.0$ is denoted as the liquefiable layer.

Buildings I and H. Due to the uniformity of the CPTs in Area 2, LS5 and LS6 can be described using a common set of CPTs which span a similar distance from north to south and are located between the two lateral spreads, as shown in Figure 24. The resulting LDI (~230 cm) shown in Figure 24 is reduced from estimates of those LS sites along the seawall. This contributed to the reduced thickness of the liquefiable sandy layer. As noted by Bassal et al. (2024) the mechanisms of extensional ground cracking at the LS 5,6, and 7 transects are complex as they were measured between rows of buildings that settled. The ground cracks may have been induced entirely or partially by ground settlement rather than seaward spreading.

Critical layers for level ground sites

The İskenderun level ground case histories are well-constrained by the seismic demand of the M_w 7.8 Kahramanmaraş earthquake utilizing ground motion recordings, subsurface data through several CPTs, and observations of ground failure (i.e. ejecta). The critical layer for each level ground site case history is selected utilizing the approach of Dhakal et al. (2020), which is similar to that of Green et al. (2014). The critical layer is the soil layer that would have most likely liquefied early during earthquake shaking and produced manifestations of liquefaction if it had occurred. Thick sand to silty sand units likely liquefied at these sites in İskenderun as indicated in Figure 10, 13, 16, 18, and 19. The weakest, shallowest soil layer within these soil units which was sufficiently thick to produce ejecta is selected as the critical layer at these sites. Profiles of Q_{tn}, I_c, FS_{liq}, and S_v (e.g. see

Table 2. Summary of critical layer properties for level ground sites.

Site	Liquefaction manifestation	PGA (g)[a]	Water Depth (m)[b]	Critical Depth Interval (m)	σ'_v at Midpoint (MPa)	Geomean CSR[c]	Geomean q_t (MPa) [COV]	Geomean f_s (MPa) [COV]	Geomean Q_{tn}	Geomean I_c
Area 1	Yes	0.33 [0.27–0.41]	1.5	3.3–5.0	0.041	0.30	5.20 [0.36]	0.031 [0.50]	81	1.86
Area 2	Yes	0.33 [0.27–0.41]	1.5	3.3–5.0	0.047	0.30	5.88 [0.31]	0.038 [0.42]	90	1.83
Area 3A	Yes	0.32 [0.26–0.39]	1.5	3.5–4.7	0.048	0.30	7.44 [0.13]	0.038 [0.16]	112	1.70
Area 3B	Yes	0.32 [0.26–0.39]	1.5	3.8–5.0	0.051	0.31	6.46 [0.20]	0.054 [0.55]	105	1.86
Area 4	Yes	0.32 [0.28–0.37]	1.5	4.3–9.0	0.069	0.34	7.73 [0.23]	0.049 [0.52]	101	1.79
Area 5A	Yes	0.32 [0.28–0.37]	1.5	3.8–7.0	0.057	0.32	6.95 [0.31]	0.046 [0.24]	96	1.81
Area 5B	Yes	0.32 [0.28–0.37]	1.5	2.0–3.3	0.032	0.26	5.20 [0.21]	0.019 [0.39]	86	1.73
SMS 3112	No[d]	0.32 [0.28–0.37]	1.5	2.9–3.5	0.038	0.28	8.17 [0.20]	0.045 [1.56]	133	1.69

Notes: Observations and seismic demand parameters are of the M_w 7.8 event; Inferred soil type is Sand to Silty Sand based on I_c; Unit weight of fill is estimated as 20 kN/m^3.

[a]Reported as mean and [16%–84%] percentiles.

[b]Water Depth refers to estimated depth during earthquake.

[c]CSR = cyclic stress ratio.

[d]At SMS 3112, no ground failure manifestations were observed within ~100 m.

Figure 10), among other parameters, were examined. The critical layer is the relatively shallow soil layer of sufficient thickness to produce ejecta which has fairly consistent soil behavior type index and penetration resistance values.

The key properties of the critical layers selected in this study are summarized in Table 2. For areas where there was a transition in the subsurface conditions within the area, as indicated by the CPT profiles, two sites are used. In Area 3, CPT10 indicated a homogeneous sandy layer from 3 to 11 m. However, CPT39 to the south of CPT10 had a 1.5-m thick clay layer at a depth of 5 m. Based on these different profiles and the transition profiles depicted by intermediate CPTs 38 and 40, Area 3 was divided into sites 3A (CPT10) and 3B (CPT39), with each site having different critical layers. For Area 5, the eastern most CPT (44) lacks a dense upper sand layer ($Q_{tn} \geqslant 200$) that is present in the three western CPTs (46, 12, and 43). Thus Area 5 is split into sites 5aA (CPTs 46, 12 and 43) and 5B (CPT44). The information in Table 2 can be used in future efforts such as assessing liquefaction triggering procedures, site response analyses, and effective stress soil-structure interaction analyses at the building sites discussed in this study.

Conclusion

The 2023 Kahramanmaraş earthquake caused extensive damage in the port city of İskenderun due to liquefaction. A comprehensive field investigation using 40 CPTs and 7 SCPTs was conducted to characterize the subsurface conditions at several building settlement and lateral spread sites and a seismic station surveyed after the earthquake. The site investigations and subsequent liquefaction assessments reveal the reclaimed shoreline area has a consistent subsurface profile with a dense gravelly fill layer overlying a thick layer of liquefiable sand, followed by interbedded silt and sand, which is followed by a thick clay deposit. Recorded ground motions and a kriging approach provided the basis for estimating intensity measures such as PGA, CAV, and Sa(1s) that are used for liquefaction assessments. By documenting these subsurface conditions and providing estimates of ground motion intensity measures, this study provides the missing

components of the Moug et al. (2024a) and Bassal et al. (2024) studies that captured ground and building deformation data to realize high-quality liquefaction field case histories in İskenderun.

The reclaimed shoreline area, which exhibited the most significant liquefaction effects, is characterized by a thick deposit of saturated medium dense sand and silty sand layers prone to liquefaction. It is not surprising these sandy layers liquefied during the 2023 Kahramanmaraş earthquake. However, there were significant differences in the liquefaction-induced building settlements in the areas studied, ranging from less than 1 to 74 cm. The large range of settlements highlights the importance of adjacent building interactions during earthquakes and its potential impact on ground deformations. Hence, these field case histories of liquefaction-induced building settlement provide the opportunity to evaluate and improve liquefaction assessment procedures. The well-documented lateral spreading field case histories also provide important data to refine empirical procedures to estimate lateral spread ground displacements and to develop new analytical procedures to model displacement patterns. Finally, critical layer interpretations and liquefaction manifestations are summarized for updating liquefaction triggering procedures.

Acknowledgments

Any opinions, findings, conclusions, or recommendations expressed in this material are those of the authors and do not necessarily reflect the views of the NSF. Any use of trade, firm, or product names is for descriptive purposes only and does not imply endorsement by the U.S. Government. Researchers from the Middle East Technical University received support from the Turkish government. The field work was conducted in coordination with Zemin Etüd ve Tasarım AŞ, a Turkish geotechnical engineering company. In particular, a GEER team member, Sena Begüm Kendır, and Dr H Turan Durgunoğlu provided guidance and logistical support to the team. We also sincerely thank TC Antakya Kaymakamlığı for their valuable assistance and support.

Declaration of conflicting interests

The authors declared no potential conflicts of interest with respect to the research, authorship, and/or publication of this article.

Funding

The authors disclosed receipt of the following financial support for the research, authorship, and/or publication of this article: This research is supported by the National Science Foundation (NSF) through the Engineering for Civil Infrastructure Program under grant no. CMMI 2338023, 2338024, 2338025, and 2338026. It also takes advantage of data collected through the NSF-supported GEER Association under Grant No. CMMI1826118.

ORCID iDs

Cody Arnold https://orcid.org/0009-0008-0764-7153
Patrick Bassal https://orcid.org/0000-0003-4153-2460
Chenying Liu https://orcid.org/0000-0001-5183-4265

Data availability statement

Some or all the data on post-event observations included in this publication are available at DesignSafe DOI: https://doi.org/10.17603/ds2-q5x1-e497 (Moug et al., 2024b). In addition, all geo-

located field-testing data reported in this study are available at DesignSafe DOI: https://doi.org/10.17603/ds2-6473-fs88 (Macedo et al., 2025).

References

Bassal P, Papageorgiou E, Moug D, Bray J, Cetin K, Şahin A, Kubatko E, Nepal S, Toth C, Kendır S and Bikce M (2024) Liquefaction ground deformations and cascading coastal flood hazard in the 2023 Kahramanmaraş earthquake sequence. *Earthquake Spectra* 40: 247830.

Boore DM, Stewart JP, Seyhan E and Atkinson GM (2014) NGA-West2 equations for predicting PGA, PGV, and 5% damped PSA for shallow crustal earthquakes. *Earthquake Spectra* 30(3): 1057–1085.

Boulanger R and Idriss I (2014) *CPT and SPT based liquefaction triggering procedures*. Report no: UCD/CGM-14/01. Davis, CA: Center for Geotechnical Modeling, University of California, Davis.

Bradley B and Hughes M (2012) Conditional peak ground accelerations in the Canterbury earthquakes for conventional liquefaction assessment - Part 1. *Technical Report Prepared for the Ministry of Business, Innovation and Employment*. April 2012. 22p.

Bray J and Macedo J (2017) 6th Ishihara lecture: Simplified procedure for estimating liquefaction induced building settlement. *Soil Dynamics and Earthquake Engineering* 102: 215–231.

Bray JD and Olaya FR (2023) 2022 H. Bolton seed memorial lecture: Evaluating liquefaction effects. *Journal of Geotechnical and Geoenvironmental Engineering*, ASCE 149(8): 11242.

Buckreis T, Pretell R, Sandikkaya M, Kale O, Askan A, Brandenberg S and Stewart J (2024) Engineering attributes of ground motions from February 2023 Türkiye earthquake sequence. *Earthquake Spectra* 40: 2268–2284.

Cetin K, Bray J, Frost J, Hortacsu A, Miranda E, Moss R and Stewart J (2023) *February 6, 2023 Türkiye earthquakes: Report on geoscience and engineering impacts*. GEER Association report 082, 6 May. Oakland, CA: Earthquake Engineering Research Institute.

Denge Mühendislik Ltd. Sti (2011) Hatay Ili—İskenderun Ilcesi—İskenderun Belediyesi Mikrobolgeleme Etud Raporu

Dhakal R, Cubrinovski M and Bray JD (2020) Geotechnical characterization and liquefaction evaluation of gravelly reclamations and hydraulic fills (port of Wellington, New Zealand). *Soils and Foundations* 60: 1507–1531.

Eryılmaz M and Eryılmaz FY (2003) Recent surface sediment distribution of İskenderun Bay. In: *Proceedings of 56th geological congress of Turkey*, Ankara, Turkiye, pp. 286–287.

Google (n.d.) Southeastern Türkiye. Available at: https://mt1.google.com/vt/lyrs=s&x=x&y=y&z=z (accessed 12 March 2024).

Green RA, Cubrinovski M, Cox B, Wood C, Wotherspoon L, Bradley B and Maurer B (2014) Select liquefaction case histories from the 2010–2011 Canterbury earthquake sequence. *Earthquake Spectra* 30: 131–153.

Hutabarat D and Bray J (2022) Estimating the severity of liquefaction ejecta using the cone penetration test. *Journal of Geotechnical and Geoenvironmental Engineering* 148: 2744.

Jayaram N and Baker JW (2009) Deaggregation of lifeline risk: Insights for choosing deterministic scenario earthquakes. In: *Proceedings TCLEE2009 conference: Lifeline earthquake engineering in a Multihazard environment*, Oakland, CA, 26 April.

Jayaram N and Baker JW (2010) Efficient sampling and data reduction techniques for probabilistic seismic lifeline risk assessment. *Earthquake Engineering & Structural Dynamics* 39: 1109–1131.

Karabacak V, Özkaymak Sözbilir ÇH, Tatar O, Aktuğ B, Özdağ ÖC, Çakir R, Aksoy E, Koçbulut F, Softa M, Akgün E, Demir A and Arslan G (2023) M_w The 2023 Pazarcık (Kahramanmaraş, Türkiye) earthquake (7.7): Implications for surface rupture dynamics along the East Anatolian fault zone. *Journal of the Geological Society* 180(3): jgs2023020.

Macedo J, Bray J, Moug D, Bassal P and Arnold C (2025) Subsurface characterization of İskenderun—2024 in subsurface characterization of selected liquefaction case histories: 2023 Kahramanmaraş earthquake sequence. *DesignSafe-CI*. DOI: 10.17603/ds2-6473-fs88.

Moug D, Bassal P, Bray J, Cetin K, Kendir S, Şahin A, Cakir E, Soylemez B and Ocak S (2023) *February 6, 2023 Türkiye earthquakes: GEER phase 3 team report on selected geotechnical engineering effects*. GEER Association Report 082-S1, June 30. Ankara: Middle East Technical University.

Moug D, Bray J, Bassal P, Macedo J, Ulmer K, Cetin K, Kendir S, Şahin A, Arnold C and Bikçe M (2024a) Liquefaction-induced ground and building interactions in İskenderun from the 2023 Kahramanmaraş earthquake sequence. *Earthquake Spectra* 40(2): 913–938.

Moug D, Bray J, Bassal P, Şahin A and Kendır S (2024b) Lidar scans of liquefaction-impacted buildings in İskenderun, Hatay in GEER Lidar data from the 2023 Kahramanmaraş earthquake eequence reconnaissance. *DesignSafe-CI*. DOI: 10.17603/ds2-q5x1-e497.

Nalça C (2018) *Transformation of İskenderun historic urban fabric from mid-19th century to the end of the French mandate period*. Master's Thesis, Department of Architectural Restoration, Izmir Institute of Technology, Izmir.

Okay HB and Özacar AA (2023) A novel VS30 prediction strategy taking fluid saturation into account and a new VS30 model of Türkiye. *In Bulletin of the Seismological Society of America* 114(2): 1048–1065.

Özdemir A, Yasxar E and Şahinoglu A (2019) Geothermal geophysical studies in İskenderun (Hatay): The first indication for geothermal energy. In: *Proceedings of the 3rd international symposium on multidisciplinary studies and innovative technologies*, Ankara, Turkiye, pp. 11–13.

Özener P, Monkul MM, Bayat EE, Ari A and Cetin KO (2024) Liquefaction and performance of foundation systems in İskenderun during 2023 Kahramanmaras-Turkiye earthquake sequence. *Soil Dynamics and Earthquake Engineering* 178: 108433.

Öztürk H, Davis CA, Kuşku Dalğiç İS, Kasapçi C and Şengül MA (2024) M_wM_w soil liquefaction and subsidence disaster in İskenderun related to the 6 February 2023 Pazarcık (: 7.7) and 20 February Defne (: 6.4) earthquakes, Türkiye. *Turkish Journal of Earth Sciences* 33(1): 7.

Reitman N, Briggs R, Barnhart W, Jobe J, DuRoss C, Hatem A, Gold R, Mejstrik J and Akçiz S (2023) Preliminary fault rupture mapping of the 2023 Mw7.8 and Mw7.5 Türkiye earthquakes. *Earthquake Research Advances* 4: 100219.

Robertson P (2009) Performance-based earthquake design using the CPT. In: Kokusho T, Tsukamoto Y and Yoshimine M (eds) *Earthquake Geotechnical Engineering: From Case History to Practice*. London: Taylor & Francis, pp. 3–20.

Robertson PK and Wride CE (1998) Evaluating cyclic liquefaction potential using the cone penetration rest. *Canadian Geotechnical Journal* 35(3): 442–459.

Taftsoglou M, Valkaniotis S, Papathanassiou G and Karantanellis E (2023) Satellite imagery for rapid detection of liquefaction surface manifestations: The case study of Türkiye-Syria 2023 earthquakes. *Remote Sensing* 15: 4190.

van Ballegooy S, Malan P, Lacrosse V, Jacka M, Cubrinovski M, Bray J, O'Rourke T, Crawford S and Cowan H (2014) Assessment of liquefaction-induced land damage for residential Christchurch. *Earthquake Spectra* 30: 31–55.

Wang Z, Zhang W, Taymaz T, He Z, Xu T and Zhang Z (2023) Dynamic rupture process of the 2023 M_w 7.8 Kahramanmaraş earthquake (SE Türkiye): Variable rupture speed and implications for seismic hazard. *Geophysical Research Letters* 50(15): e2023GL104787.

Zhang G, Robertson P and Brachman R (2002) Estimating liquefaction-induced ground settlements from CPT for level ground. *Canadian Geotechnical Journal* 39: 1168–1180.

Zhang G, Robertson PK and Brachman RWI (2004) Estimating liquefaction-induced lateral displacements using the standard penetration test or cone penetration test. *Journal of Geotechnical and Geoenvironmental Engineering* 130: 861–871.

Appendix I

Table 3. Summary of liquefaction indices at building settlement sites (16%–84%, for areas with more than two CPTs).

Site	Observed settlement (cm)	SV (cm)	LBS	LSN	LD	Consistency with field observations
Area 1	47–71	16–25	23–35	25–33	40–80	Yes—High indices align with large building settlements and significant ejecta.
Area 2	22–51	15–22	23–31	27–30	55–110	Yes—High indices align with large building settlements and significant ejecta.
Area 3A	45–50	29	44	38	65	Yes—High indices align with large building settlements and significant ejecta.
Area 3B	0	24	37	32	36	No—High indices do not align with low building settlement and lack of ejecta.
Area 4	6	23 & 27	34 & 39	28 & 34	42 & 88	No—High indices do not align with low building settlement and lack of ejecta.
Area 5A	30–37	25–26	40–62	33–39	60–90	Yes—High indices align with large building settlements and significant ejecta.
Area 5B	7–16	32	49	53	73	Mixed—High indices do not align with low building settlements. High indices align with significant ejecta.